JOURNAL OF MODERN OPTICS, 2017
http://dx.doi.org/10.1080/09500340.2017.1288838

Taylor & Francis
Taylor & Francis Group

Trapping field assisted backscattering in strong-field photoemission from dielectric nanospheres

Lennart Seiffert[a], Philipp Henning[a], Philipp Rupp[c,d], Sergey Zherebtsov[c,d], Peter Hommelhoff[b], Matthias F. Kling[c,d] and Thomas Fennel[a,e]

[a]Institut für Physik, Universität Rostock, Rostock, Germany; [b]Department Physik, Friedrich-Alexander-Universität Erlangen-Nürnberg, Erlangen, Germany; [c]Max-Planck-Institut für Quantenoptik, Garching, Germany; [d]Physik Department, Ludwig-Maximilians-Universität München, Garching, Germany; [e]Max-Born-Institut für Nichtlineare Optik und Kurzzeitspektroskopie, Berlin, Germany

ABSTRACT

We study strong-field ionization of dielectric nanospheres and focus on the enhancement of the cut-off energies for backscattering electrons resulting from charge interaction. Though recent studies clearly demonstrated the decisive impact of a surface trapping field on the electron backscattering process, a clear picture of the underlying mechanism is lacking. Here, we provide this picture and present a simple and transparent extension of the famous three-step model of strong-field science by adding a triangular surface trapping potential. We justify this model for the case of dielectric nanospheres based on high-level transport simulations. The analysis of the trapping field assisted backscattering provides a universal scaling of the maximal recollision and backscattering energies as 9 U_p and 14.5 U_p, respectively, where U_p is the local ponderomotive potential. The universal nature of the enhancement over the conventional three-step model is of particular interest for the generation of attosecond electron bunches via near-field induced photoemission and high harmonic generation at nanostructures.

ARTICLE HISTORY
Received 15 October 2016
Accepted 16 January 2017

KEYWORDS
Strong-field ionization; electron backscattering; nanostructures; near-fields; dielectric nanospheres

1. Introduction

When an atom or molecule is exposed to a strong laser pulse, electrons can (i) be released by tunnelling or multi-photon ionization, (ii) be accelerated in the laser field and (iii) recollide with the residual ion to recombine under the emission of an energetic photon or to scatter elastically and escape. This simplified scheme, often referred to as the simple man's model (SMM) or the three-step model of strong-field physics (*1*), not only provides a clear picture of the physics underlying high-harmonic generation (HHG) (*2*), attosecond pulse generation (*3*) and high-order above-threshold ionization (HATI) (*4*) but also yields a useful estimate of the prevailing cut-off features in the respective emission spectra. In particular, the 3.17 U_p cut-off in HHG and the 10 U_p cut-off in HATI can be linked to the maximal recollision energy and optimal elastic backscattering, respectively. The relevant energy scale is the ponderomotive potential $U_p = e^2E_0^2/4m\omega^2$, where E_0 and ω are the electric field amplitude and angular frequency of the incident laser field and e and m are the elementary charge and electron mass, respectively. Classical or quantum trajectories, as often used within the so-called strong-field approximation and its generalizations (*5*, *6*), are the key tool for analyzing the effects of waveform-controlled pulses (*4*), multicolour fields (*7*, *8*) and bicircular laser pulses (*9*, *10*) on atomic and molecular strong-field processes.

Sparked by several pioneering experiments (*11*–*13*), the strong-field physics of nanostructures and nanostructured solids has received considerable attention over the last few years. One key motivator for this development is the fact that the illumination of nanostructures creates near-fields that can be strongly enhanced with respect to the incident field and localized on dimensions far below the wavelength. Control of electronic motion with such localized fields is of particular interest for light-wave driven nanoelectronics. Several concepts of atomic and molecular strong-field physics have been demonstrated for nanostructures. For example, as for HATI in atoms, electron backscattering of tunnel electrons at the surface of laser driven nanostructures was found to be the dominant acceleration process for the high-energy photoemission from dielectric nanospheres (*11*), metal nanotips (*12*, *13*) and surface-assembled nanoantennas (*14*). Multiple experiments could demonstrate waveform control via the carrier-envelope phase (*11*, *12*, *14*, *15*), justifying the recollision picture via the observed phase-dependent features for the most energetic electrons.

CONTACT Thomas Fennel thomas.fennel@uni-rostock.de

However, besides the expected higher cut-off energies due to the field enhancement (*16*), the strong-field photoemission from nanostructures also turned out to feature substantial new effects. First, the finite range of the near-field becomes an active parameter in the dynamics. If the electron's quiver amplitude exceeds the decay length of the field enhancement, recollision can be quenched completely (*13*, *17*). Second, the charge interaction among the released electrons and with residual ions at the nanostructure's surface was found to substantially enhance the photoemission cut-offs for dielectric nanospheres (*11*, *18*). Third, field propagation (*19*) and vectorial field effects (*20*) were found to have pronounced impact on the directionality and nature of the electron emission. The near-field deformation due to field propagation modifies the angular distribution of photoelectrons, opening routes for all-optical directional control. Particularly, strong tangential field components can further lead to a qualitative change, as double recollisions can become dominant under appropriate conditions (*21*).

Here, we focus on the physics of the second effect, i.e. the cut-off enhancement due to charge interaction. In fact, in earlier works, the presence of enhanced emission energies due to (i) a local trapping potential in the vicinity of the surface and (ii) Coulomb explosion in the escaping electron bunch resulting from space charge repulsion have been clearly identified. A clear analysis of the important stages of the mechanism and the scaling, however, is still lacking. This defines the scope of the current theoretical study. Motivated by the analysis of a simulation for a typical reference scenario, we analyze the effect of an attractive short-range trapping field on the backscattering cut-off for a triangular trapping potential. Our analysis reveals a universal scaling of enhancement and identifies the relevant step that leads to the dominant energy gain. In particular, we find that the trapping diminishes the energy of directly emitted electrons, results in a maximal backscattering cut-off of $\approx$14.5 U_p, and a maximum recollison energy of $\approx$ 9 U_p, enabling prediction of possible future enhanced HHG from dielectric nanosystems.

2. The reference scenario

As a reference scenario, we consider the photoemission from small ($d \ll \lambda$) silica spheres in a near-infrared (NIR) few-cycle laser pulse. In this case, the near-fields exhibit hot spots at the particle poles, see Figure 1(a). To model the strong-field ionization of the dielectric nanospheres and the subsequent electron emission, we employed the semi-classical Mean-field Mie Monte-Carlo (M^3C) model as described in detail in Refs. (*19*, *21*). In brief, electron trajectories are generated via tunnel ionization (evaluated using the ADK tunnelling rate (*22*) and an effective ionization potential of $I_p = 9$ eV to describe the band-gap of SiO_2) outside the sphere surface and propagated in the near-field by integration of classical equations of motion. The near-field is constructed from the Mie solution (*23*), which represents the pure linear-response result, and an effective mean-field resulting from free charges. The latter contribution contains both, the Coulomb interaction between the free charges and the additional polarization of the sphere due to their presence, both in electrostatic approximation. For trajectories propagating inside the material, we account for elastic electron-atom scattering and inelastic electron–electron scattering via effective mean-free paths, extracted from quantum scattering calculations for the atomic potentials and from semi-classical Lotz cross sections (*24*), respectively, and evaluated via Monte-Carlo methods. We count electrons outside of the sphere as emitted when they have (i) a positive single-particle energy and (ii) an outgoing momentum, both evaluated sufficiently late in the simulation to ensure convergence.

Figure 1 shows the results for a typical reference scenario, see e.g. Refs. (*11*, *19*). We consider a SiO_2 nanosphere with diameter $d = 100$ nm under a $\lambda = 720$ nm near-infrared 4 fs (full width at half maximum of the intensity envelope) pulse at peak intensity $I_0 = 3 \times 10^{13}$ Wcm^{-2} and with carrier envelope phase $\varphi_{ce} = 0$ (cosine pulse). Near-field driven tunnelling and the subsequent separation of electrons and residual ions at the surface yields a capacitor field that we term the trapping field, see Figure 1(a). The latter, which has a range on the order of the quiver amplitude, attracts electrons to the surface and confines a substantial portion of the conduction electrons. Surprisingly, though the trapping field diminishes direct electrons, it enhances the energy gain for backscattering. Further, the bunch of backscattered electrons emitted in a given half cycle experiences space charge repulsion that leads to Coulomb explosion and, therefore, causes spectral broadening of the photoelectron distribution and further acceleration of a portion of the electrons. This represents the second mechanism for charge interaction supported energy gain.

The combined impact of the above two effects yields a sizable cut-off enhancement, as shown by comparison of electron spectra calculated with and without the mean-field in Figure 1(b). Besides the quenching of direct emission (compare dashed red to dashed black curve), charge interaction enhances the cut-off from backscattered electrons by almost 50% (red arrow). The deviation of the cut-off extracted without mean-field (black dot) from the 10 U_p SMM result is attributed to the finite tunnel exit. In the simulation, the two different charge interaction supported acceleration effects can be

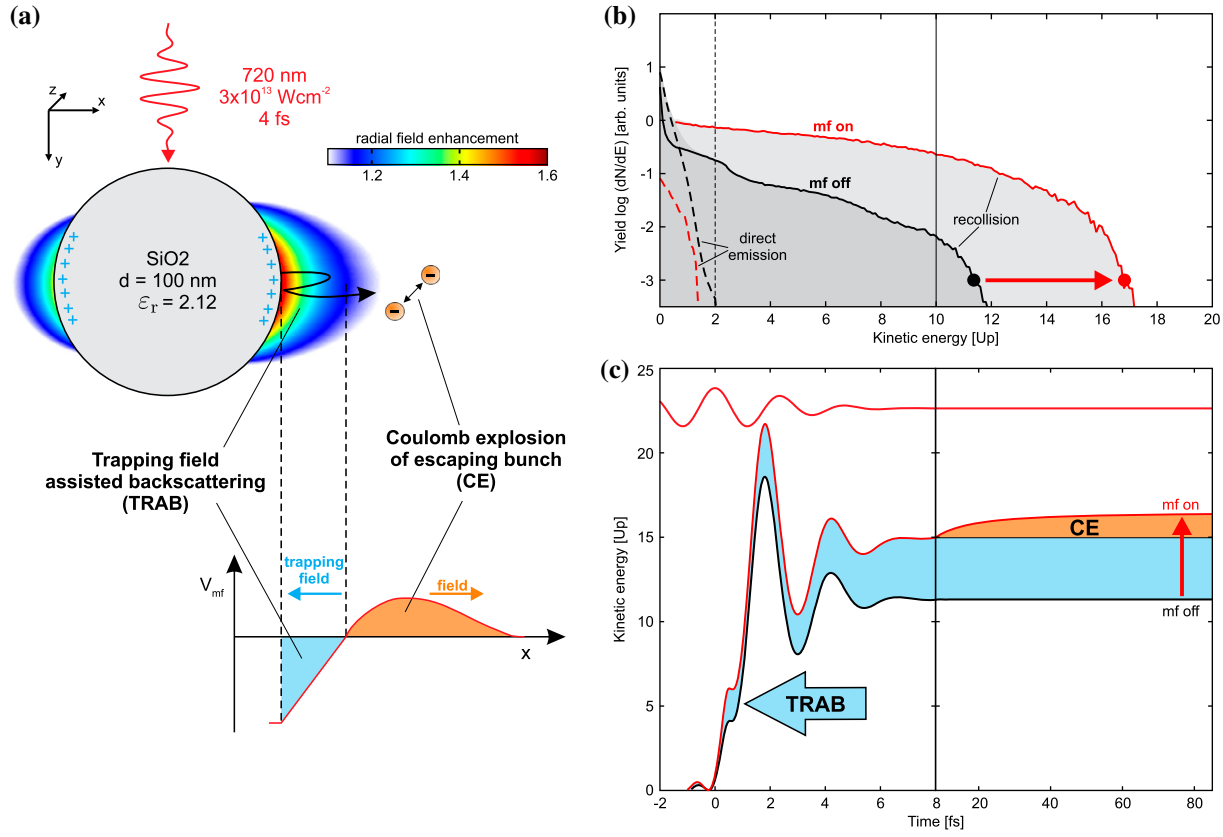

Figure 1. Strong-field photoemission from a dielectric nanosphere. (a) Maximum field enhancement at a $d = 100$ nm SiO_2 nanosphere excited by a near-infrared few-cycle pulse (parameters as indicated). Blue plus symbols indicate the positive surface charge induced by the residual ions resulting from tunnel ionization in the enhanced surface field. The orange spheres represent a bunch of emitted backscattered electrons (see schematic trajectory) that Coulomb explode due to space charge repulsion. Inset: Schematic potential induced by the free charges leading to an attractive trapping potential (blue) near the surface and a repulsive component in the bunch (orange). (b) Energy spectra of emitted electrons from simulations excluding (black curves) and including (red curves) charge interaction. Grey areas represent full spectra, dashed and solid lines show selective spectra for directly emitted electrons and backscattered electrons, respectively. The cut-offs (symbols) are defined as the energies where the backscattering spectra drop by three orders of magnitude. Vertical lines indicate the classical $2\,U_p$ and $10\,U_p$ cut-offs for direct emission and backscattering, respectively. (c) Time evolution of the kinetic energies for representative trajectories corresponding to the respective cut-off energies. The blue area indicates the energy difference resulting from the trapping field (blue arrow). The orange area shows the additional energy accumulated during the escape phase due to Coulomb explosion of the escaping electron bunch (CE).

separated as they develop on very different timescales. This is demonstrated in Figure 1(c), where the evolution of the kinetic energies is compared for two representative trajectories corresponding to the respective cut-off energies (cf. black and red dots in Figure 1(b)). The first jump of the energy during the recollision process is attributed to the trapping field assisted backscattering (TRAB) (blue arrow and area), while the second energy gain takes place on a longer timescale and is attributed to the Coulomb explosion of the escaping electron bunch (orange area). Note that the quantitative separation of the two effects is possible via analysis of the energy gains from the different contributions to the local near-fields (*19*).

Having identified the clear separation of the effects via their timescales, we are able to assign the relevant regions of the mean-field potential (Figure 2(b)) to the acceleration effects. The mean-field potential $V_{\mathrm{mf}} = -e\Phi_{\mathrm{mf}}$ characterizes the electron potential energy resulting from the scalar electric potential Φ_{mf}. The electron density evolution in Figure 2(a) shows the build-up of the underlying charge separation at the surface as well as the escaping fast electrons. First, the negative potential (blue) represents the attractive trapping field induced by the positively charged surface (Figure 2(b)). Second, the region of positive potential (red) indicates the space charge repulsion among the emitted electrons that unfolds on the longer timescale and thus only acts like a potential offset in the early stages. This justifies to focus on the fast dynamics that is connected to the trapping field and the corresponding energy enhancement, see red rectangle and Figure 2(c). Altogether, the extracted mean-field leads to a potential profile as sketched in Figure 1(a). The accordingly zoomed region of the mean-field in Figure 2(c) and the trajectories corresponding to the cut-off energies

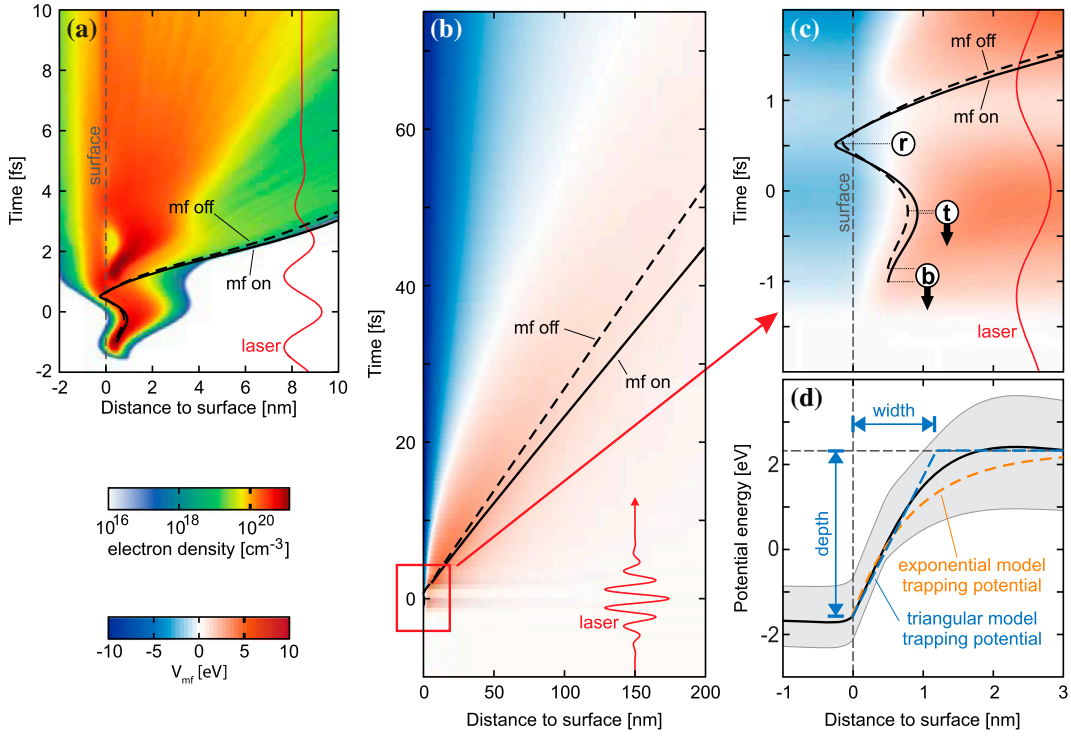

Figure 2. Evolution of the charge interaction induced mean-field. (a) Time evolution of the electron density along the polarization axis (x axis). Dashed and solid black curves show backscattering trajectories of the electrons from Figure 1(c) excluding and including the mean-field, respectively. (b) Corresponding evolution of the mean-field potential $V_{\mathrm{mf}}(x,t)$ along with the trajectories shown in (a). (c) Magnified view of the backscattering process during the dominant cycle of the laser field, see red rectangle indicated in (b) and red arrow. Labelled circles indicate the birth 'b', the outer turning point 't' and the recollision 'r'. Arrows on the circles indicate the direction of the changes in the timing when including the mean-field. (d) Mean-field potential averaged during the recollision phase, i.e. in the time interval between −1 and 1 fs. The grey area indicates the variation of the potential in this time interval and the blue and orange curves indicate triangular and exponential model trapping potentials, respectively.

(cf. Figure 1(b)) define the relevant spatiotemporal range that has to be analyzed. Note that the general evolution of the cut-off trajectories with and without mean-field remains similar, though the result with mean-field exhibits a slightly earlier birth time and a larger excursion. Most importantly, during the relevant time interval, the trapping potential varies only little and exhibits an overall shape similar to a triangular potential barrier (see Figure 2(d)). This motivates our ansatz to model the trapping potential as a static triangular barrier (dashed blue curve) for the following trajectory analysis.

3. Trapping field assisted backscattering

For the systematic analysis of the trapping field effect, we calculate one-dimensional electron trajectories that start at rest from the origin (surface) in the presence of the effective field containing the laser and the trapping field barrier via integration of the classical equation of motion (EOM)

$$\ddot{x}(t) = -\frac{e}{m}\mathcal{E}_0\left[f(t)\cos\left(\omega t\right) + \epsilon(x)\right]. \tag{1}$$

Here, $f(t)$ is the normalized field envelope and $\epsilon(x)$ characterizes the field resulting from the barrier. This equation of motion can be made general by introducing the scaled displacement $\xi = x/x_{\mathrm{q}}$, where $x_{\mathrm{q}} = \frac{e\mathcal{E}_0}{m\omega^2}$ is the quiver amplitude, and the scaled time $\tau = \omega t$. The resulting EOM reads

$$\ddot{\xi}(\tau) = -\left[f(\tau)\cos(\tau) + \epsilon(\xi)\right]. \tag{2}$$

Note that the corresponding reduced kinetic energy is $\dot{\xi}^2/2$ and the ponderomotive potential is 1/4, i.e. independent of all laser parameters. A triangular barrier with field strength ϵ_0 and extension α leads to

$$\epsilon_{\mathrm{tri}}(\xi) = \begin{cases} \epsilon_0 & \text{if } \xi < \alpha \\ 0 & \text{otherwise.} \end{cases} \tag{3}$$

Alternatively, one may also consider an exponential barrier with trapping field shape $\epsilon_{\mathrm{exp}}(\xi) = \epsilon_0 \exp(-\xi/\alpha)$. For trajectories returning to the surface within a full laser cycle, we assume elastic backscattering. As a result, each trajectory is fully characterized by its reduced birth time as this determines if the trajectory corresponds to a

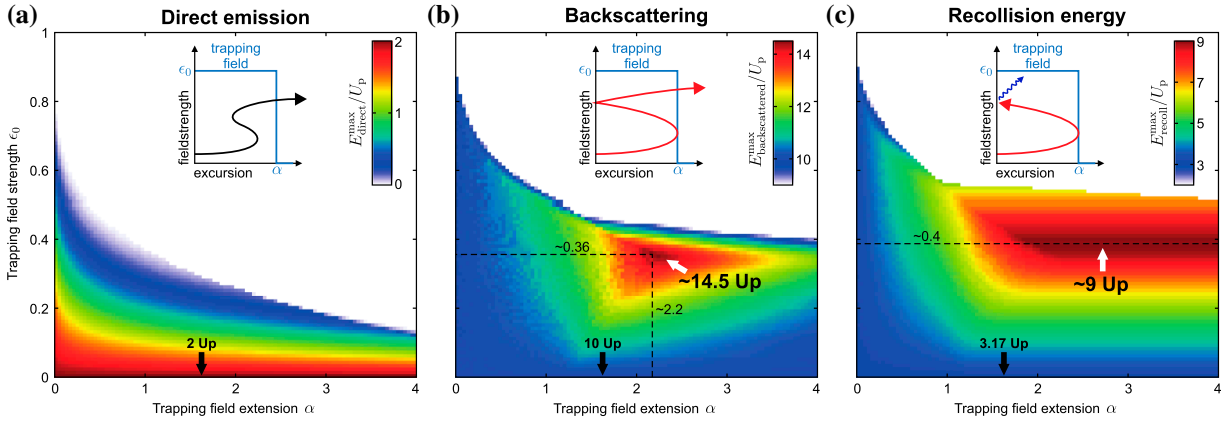

Figure 3. Trapping field induced quenching and enhancement of the electron emission from surfaces. (a), (b) Final energies of optimal trajectories for directly emitted (a) and backscattered (b) electrons as function of the extension α and strength ϵ_0 of the triangular potential. Energies are given in units of the ponderomotive energy. For optimal parameters, a maximum enhanced energy of $\approx$ 14.5 U_p is found for backscattering. (c) Recollision energy of critical backscattering trajectories in dependence of the trapping field as in (a) and (b). The horizontal dashed line indicates the optimal field strength for which a maximum recollision energy of 9 U_p is achieved.

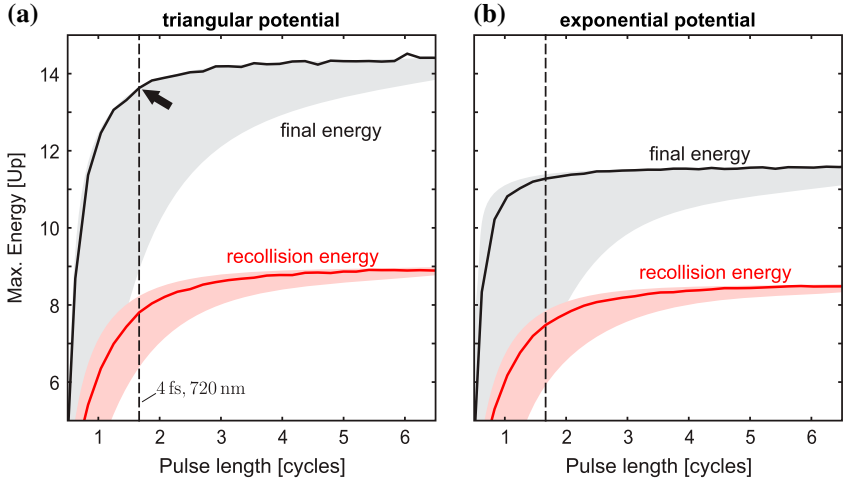

Figure 4. Pulse length dependence (a), (b) Final energies (black) and recollision energies (red) for a triangular potential (a) and an exponential potential (b) as function of pulse duration for optimal potential parameters (cf. white arrows in Figure 3(b), (c)). Solid lines represent the results for a carrier-envelope phase (CEP) of zero (cosine-like pulses). Shaded areas indicate the variation with the CEP. Note that the pulse length is measured in cycles of the laser field. The value corresponding to 4 fs at 720 nm ($\approx$ 1.7 cycles) is indicated by the vertical dashed lines.

directly emitted or backscattered electron. In our further analysis of the scaling of the photoemission cut-off, we analyze the trajectories resulting in the maximal energy for (i) direct emission and (ii) backscattering. In addition, as this would be relevant for the cut-off in HHG, we also extract (iii) the highest recollision energy.

The systematic analysis of these three characteristic cut-off energies in the case of long pulses and for the triangular barrier in Figure 3 shows the following main results. First, starting from the well-known value of 2 U_p for vanishing trapping field ($\epsilon_0 = 0$ or in the limit $\alpha \to 0$), the direct emission cut-off decreases for both, increasing strength and extension of the trapping field (Figure 3(a)). Second, for rescattered electrons (Figure 3(b)) the energies can be substantially enhanced over the classical 10 U_p cut-off ($\epsilon_0 = 0$ or $\alpha \to 0$ limits) for a large range of trapping field parameters (see triangular feature). In particular, for an optimal set of parameters (as indicated) the energies are enhanced up to a value of 14.5 U_p (white arrow). Third, for the recollision energies we find an enhancement up to 9 U_p, i.e. the conventional 3.17 U_p cut-off energy is almost tripled. This latter enhancement effect is of particular interest for nanostructure-based HHG and has been discussed previously also for the case of atomic HHG in the presence of a static electric field (*25*, *26*).

In the long pulse results in Figure 3, the variation of the pulse amplitude between the adjacent half cycles contributing to the recollision process is neglected. For few-cycle pulses (pulse lengths $\lesssim$ 3 cycles), the enhancement

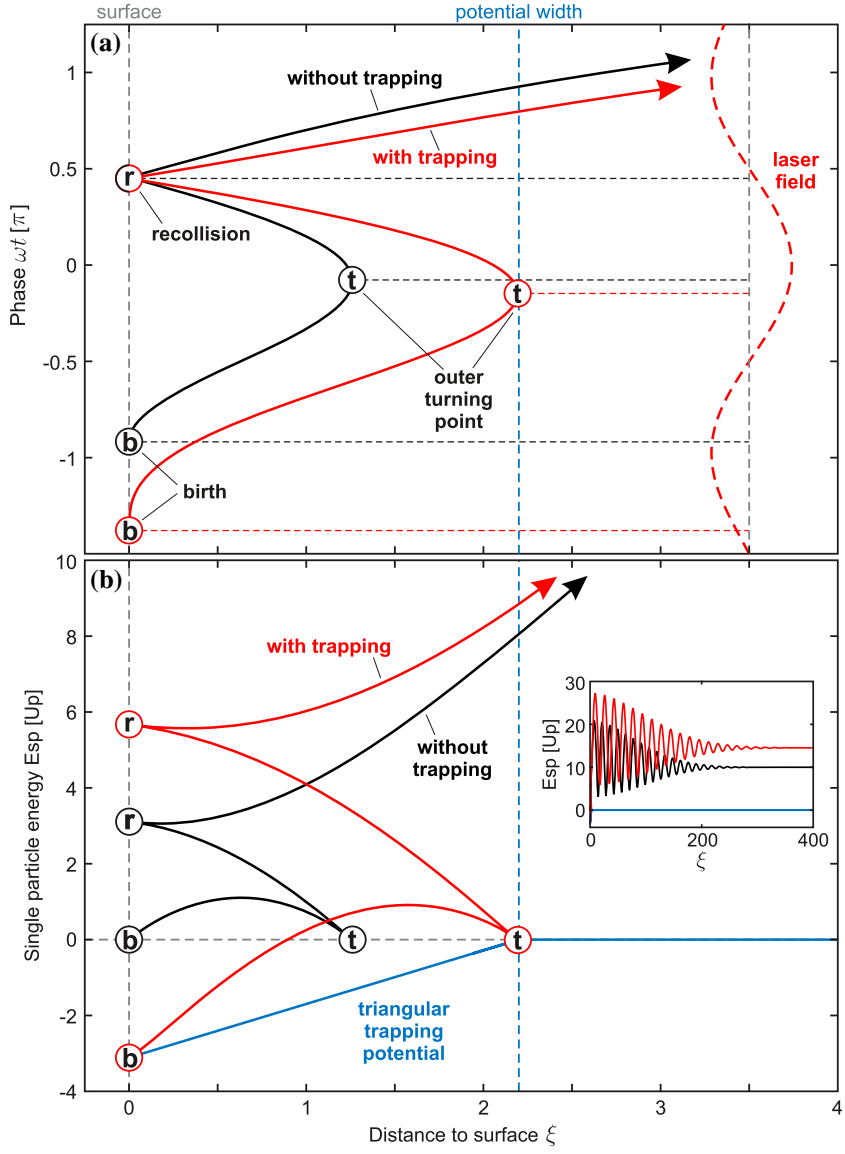

Figure 5. Trapping field assisted backscattering. (a) Optimal recollision trajectories predicted from the conventional (solid black curve) and the extended SMM, including the triangular trapping potential assuming long pulses. Labelled circles correspond to the definitions in Figure 2(c). (b) Evolution of the single-particle energies $E_{sp}(t) = E_{kin}(t) + E_{pot}(t)$ of the two trajectories shown in (a) during the recollision process. The blue curve indicates the triangular model trapping potential. The inset shows the evolution on a longer timescale for a long pulse. Vertical dashed black and blue lines indicate the surface and the trapping potential width, respectively.

becomes strongly dependent on both the pulse length and the carrier-envelope phase, see lines and shaded areas in Figure 4(a), respectively. For 4 fs pulses at 720 nm, we find an optimal backscattering cut-off of 13.7 U_p (black arrow in Figure 4(a)), i.e. an enhancement by 37%, in good agreement with the numerical results for our reference scenario in Figure 1(c) that show about 30% enhancement by the trapping field effect. This supports that the realistic backscattering process is close to realizing the optimal enhancement through TRAB. Note that the trapping field effect is further dependent on the shape of the barrier. The results for an exponential barrier in Figure 4(b) show similar recollision energies but a substantially reduced enhancement for the backscattering electrons. The latter effect is attributed to the long tail of the potential. However, the qualitative similarity of the results underlines the robustness of TRAB with respect to the potential shape.

The detailed analysis of the optimal backscattering trajectory for a triangular barrier in Figure 5 reveals the key physics of the enhancement mechanism. The comparison of the optimal trajectories in Figure 5(a) shows that the case with trapping field (red) leads to (i) an earlier birth time, (ii) a slightly earlier and (iii) more distant outer turning point when compared to the case without trapping field (black). Note that the moment of recollision is almost the same and, as expected, nearly coincides with the laser field reversal-phase $\pi/2$. The

energy analysis in Figure 5(b) shows that in both cases, the single-particle energy vanishes at the outer turning point, i.e. the turning point experiences the end of the trapping potential in the optimal case. The enhancement unfolds in the recollison process, as can be rationalized by the fact that the single-particle energy gain scales linearly with the electron velocity (as $\dot{E}_{\mathrm{sp}} = -ev\mathcal{E}_{\mathrm{las}}$ in the unscaled case, where v is the electron velocity). As the attractive potential leads to a higher velocity during approach and final departure, the electron energy gain is enhanced.

4. Conclusion

In summary, we analyzed the effect of a short-range trapping field on the strong-field photoemission from dielectric nanospheres. Motivated by a realistic reference scenario, we developed a simple and transparent model for the TRAB for a triangular potential. We extracted the universal scaling behaviour and find substantially enhanced cut-offs for both, the recollison energy and the backscattering emission cut-offs. Our results are anticipated to be of general interest for the strong-field physics of nanostructures and may be useful for the characterization and optimization of the near-field enhanced generation of attosecond electron bunches and nanostructure-based HHG.

Disclosure statement

No potential conflict of interest was reported by the authors.

Funding

This work received financial support from the DFG within SPP1840 'Quantum Dynamics in Tailored Intense fields (QUTIF)' and the Munich Centre for Advanced Photonics (MAP). L.S. and T.F. acknowledge funding within SFB 652/3 and computing time granted by the North-German supercomputing center HLRN (Project ID mvp00011). P.R., S.Z., and M.F.K. are supported by the European Union through the ERC grant ATTOCO [grant number 307203]. P.H. received funding within 'ERC grant NearFieldAtto'.

References

(1) Corkum, P.B. Plasma Perspective on Strong-Field Multiphoton Ionization. *Phys. Rev. Lett.* **1993,** *71,* 1994–1997.
(2) L'Huillier, A.; Lewenstein, M.; Salières, P.; Balcou, P.; Ivanov, M.Y.; Larsson, J.; Wahlström, C.G. High-order Harmonic-generation cutoff. *Phys. Rev. A* **1993,** *48,* R3433–R3436.
(3) Sansone, G.; Benedetti, E.; Calegari, F.; Vozzi, C.; Avaldi, L.; Flammini, R.; Poletto, L.; Villoresi, P.; Altucci, C.; Velotta, R.; Stagira, S.; De Silvestri, S.; Nisoli, M. Isolated Single-Cycle Attosecond Pulses. *Science* **2006,** *314,* 443–446.
(4) Paulus, G.G.; Nicklich, W.; Xu, H.; Lambropoulos, P.; Walther, H. Plateau in Above Threshold Ionization Spectra. *Phys. Rev. Lett.* **1994,** *72,* 2851–2854.
(5) Lewenstein, M.; Balcou, P.; Ivanov, M.Y.; L'Huillier, A.; Corkum, P.B. Theory of High-Harmonic Generation by Low-Frequency Laser Fields. *Phys. Rev. A* **1994,** *49,* 2117–2132.
(6) MiloŠević, D.B.; Bauer, D.; Becker, W. Quantum-Orbit Theory of High-Order Atomic Processes in Intense Laser Fields. *J. Modern Opt.* **2006,** *53,* 125–134.
(7) Skruszewicz, S.; Tiggesbäumker, J.; Meiwes-Broer, K.H.; Arbeiter, M.; Fennel, T.; Bauer, D. Two-Color Strong-Field Photoelectron Spectroscopy and the Phase of the Phase. *Phys. Rev. Lett.* **2015,** *115,* 043001.
(8) Kitzler, M.; Lezius, M. Spatial Control of Recollision Wave Packets with Attosecond Precision. *Phys. Rev. Lett.* **2005,** *95,* 253001.
(9) Medišauskas, L.; Wragg, J.; van der Hart, H.; Ivanov, M.Y. Generating Isolated Elliptically Polarized Attosecond Pulses Using Bichromatic Counterrotating Circularly Polarized Laser Fields. *Phys. Rev. Lett.* **2015,** *115,* 153001.
(10) Milošević, D.B. Generation of Elliptically Polarized Attosecond Pulse Trains. *Opt. Lett.* **2015,** *40,* 2381–2384.
(11) Zherebtsov, S.; Fennel, T.; Plenge, J.; Antonsson, E.; Znakovskaya, I.; Wirth, A.; Herrwerth, O.; Süßmann, F.; Peltz, C.; Ahmad, I.; Trushin, S.A.; Pervak, V.; Karsch, S.; Vrakking, M.J.J.; Langer, B.; Graf, C.; Stockman, M.I.; Krausz, F.; Rühl, E.; Kling, M.F. Controlled Near-Field Enhanced Electron Acceleration from Dielectric Nanospheres with Intense Few-Cycle Laser Fields. *Nat. Phys.* **2011,** *7,* 656–662.
(12) Krüger, M.; Schenk, M.; Hommelhoff, P. Attosecond Control of Electrons Emitted from a Nanoscale Metal Tip. *Nature* **2011,** *475,* 78–81.
(13) Herink, G.; Solli, D.R.; Gulde, M.; Ropers, C. Field-Driven Photoemission from Nanostructures Quenches the Quiver Motion. *Nature* **2012,** *483,* 190–193.
(14) Dombi, P.; Hörl, A.; Rácz, P.; Márton, I.; Trügler, A.; Krenn, J.R.; Hohenester, U. Ultrafast Strong-Field Photoemission from Plasmonic Nanoparticles. *Nano Lett.* **2013,** *13,* 674–678.
(15) Piglosiewicz, B.; Schmidt, S.; Park, D.J.; Vogelsang, J.; Groß, P.; Manzoni, C.; Farinello, P.; Cerullo, G.; Lienau, C. Carrier-Envelope Phase Effects on the Strong-Field Photoemission of Electrons from Metallic Nanostructures. *Nat. Photonics* **2014,** *8,* 37–42.
(16) Thomas, S.; Krüger, M.; Förster, M.; Schenk, M.; Hommelhoff, P. Probing of Optical Near-Fields by Electron Rescattering on the 1 nm Scale. *Nano Lett.* **2013,** *13,* 4790–4794.
(17) Echternkamp, K.E.; Herink, G.; Yalunin, S.V.; Rademann, K.; Schäfer, S.; Ropers, C. Strong-Field Photoemission in Nanotip Near-Fields: From Quiver to Sub-Cycle Electron Dynamics. *Appl. Phys. B* **2016,** *122,* 80.
(18) Zherebtsov, S.; Süßmann, F.; Peltz, C.; Plenge, J.; Betsch, K.J.; Znakovskaya, I.; Alnaser, A.S.; Johnson, N.G.; Kübel, M.; Horn, A.; Mondes, V.; Graf, C.; Trushin, S.A.; Azzeer, A.; Vrakking, M.J.J.; Paulus, G. G.; Krausz, F.; Rühl, E.; Fennel, T.; Kling, M.F. Carrier-Envelope Phase-Tagged

Imaging of the Controlled Electron Acceleration from SiO_2 Nanospheres in Intense Few-Cycle Laser Fields, New. *J. Phys.* **2012,** *14,* 075010.

(19) Süßmann, F.; Seiffert, L.; Zherebtsov, S.; Mondes, V.; Stierle, J.; Arbeiter, M.; Plenge, J.; Rupp, P.; Peltz, C.; Kessel, A.; Trushin, S.A.; Ahn, B.; Kim, D.; Graf, C.; Rühl, E.; Kling, M.F; Fennel, T. Field Propagation-Induced Directionality of Carrier-Envelope Phase-Controlled Photoemission from Nanospheres. *Nat. Commun.* **2015,** *6,* 7944.

(20) Park, D.J.; Piglosiewicz, B.; Schmidt, S.; Kollmann, H.; Mascheck, M.; Lienau, C. Strong Field Acceleration and Steering of Ultrafast Electron Pulses from a Sharp Metallic Nanotip. *Phys. Rev. Lett.* **2012,** *109,* 244803.

(21) Seiffert, L.; Süßmann, F.; Zherebtsov, S.; Rupp, P.; Peltz, C.; Rühl, E.; Kling, M.F.; Fennel, T. Competition of Single and Double Rescattering in the Strong-Field Photoemission from Dielectric Nanospheres. *Appl. Phys. B* **2016,** *122* (4), 1–9.

(22) Ammosov, M.V.; Delone, N.B.; Krainov, V.P. Tunnel Ionization of Complex Atoms and of Atomic Ions in an Alternating Electromagnetic Field. *Sov. Phys. JETP* **1986,** *64,* 1191–1194.

(23) Mie, G. Contributions to the optics of turbid media, particularly of colloidal metal solutions. *Ann. Phys.* **1908,** *330,* 377–445.

(24) Lotz, W. An Empirical Formula for the Electron-Impact Ionization Cross-Section. *Z. Phys.* **1967,** *206,* 205–211.

(25) Wang, B.; Li, X.; Fu, P. The Effects of a Static Electric Field on High-Order Harmonic Generation. *J. Phys. B: At. Mol. Opt. Phys.* **1998,** *31,* 1961–1972.

(26) Ciappina, M.F.; Pérez-Hernéndez, J.A.; Landsman, A.S.; Okell, W.; Zherebtsov, S.; Förg, B.; Schötz, J.; Seiffert, L.; Fennel, T.; Shaaran, T.; Zimmermann, T.; Chacón, A.; Guichard, R.; Zair, A.; Tisch, J.; Marangos, J.; Witting, T.; Braun, A.; Maier, S.; Roso, L.; Krüger, M.; Hommelhoff, P.; Kling, M. F.; Krausz, F.; Lewenstein, M. Attosecond Physics at the Nanoscale; doi: 10.1088/1361-6633/aa574e.